Geomechanics and Engineering, *Vol. 19, No. 1 (2019) 79-91*
DOI: https://doi.org/10.12989/gae.2019.19.1.079

Numerical analysis of offshore monopile during repetitive lateral loading

Song-Hun Chong[1a], Ho-Sung Shin[2b] and Gye-Chun Cho*[3]

[1]*Department of Civil Engineering, Sunchon National University, Republic of Korea*
[2]*Department of Civil and Environmental Engineering, University of Ulsan, Republic of Korea*
[3]*Department of Civil and Environmental Engineering, Korean Advanced Institute for Science and Technology, Republic of Korea*

(Received April 17, 2019, Revised August 19, 2019, Accepted September 9, 2019)

Abstract. Renewed interest in the long-term pile foundations has been driven by the increase in offshore wind turbine installation to generate renewable energy. A monopile subjected to repetitive loads experiences an evolution of displacements, pile rotation, and stress redistribution along the embedded portion of the pile. However, it is not fully understood how the embedded pile interacts with the surrounding soil elements based on different pile geometries. This study investigates the long-term soil response around offshore monopiles using finite element method. The semi-empirical numerical approach is adopted to account for the fundamental features of volumetric strain (terminal void ratio) and shear strain (shakedown and ratcheting), the strain accumulation rate, and stress obliquity. The model is tested with different strain boundary conditions and stress obliquity by relaxing four model parameters. The parametric study includes pile diameter, embedded length, and moment arm distance from the surface. Numerical results indicate that different pile geometries produce a distinct evolution of lateral displacement and stress. In particular, the repetitive lateral load increases the global lateral load resistance. Further analysis provides insight into the propagation of the shear localization from the pile tip to the ground surface.

Keywords: long-term monopile foundation; semi-empirical numerical scheme; terminal void ratio; shakedown; displacement evolution; soil densification

1. Introduction

The cyclic response of laterally loaded piles has recently received considerable attention with the sharp increase of offshore operations by the oil and gas industry. An offshore pile foundation that supports a drilling and production platform deviates from classic pile scenario because the offshore environment poses additional challenge of a large number of load cycles induced by wind and wave. The development of the p-y curve for modeling soil reaction was based on the semi-empirical method. The laterally loaded pile was modeled as a Winkler elastic beam supported by nonlinear soil springs (Reese *et al.* 1974). The full-scale tests under both static and cyclic lateral loads recognized the limitation of theoretical formulation, and thus input parameters of p-y curve were modified to adjust the relative density and cyclic load effect (Reese and Cox 1975, API 1993).

A renewed interest in long-term pile foundations has also been driven by an increase in offshore wind turbines to generate renewable energy. The design of an offshore foundation mainly depends on the water depth, sediment properties, loading types, and available construction method. Among offshore foundations types, including gravity bases, suction caissons, and tripods, the monopile has been the most commonly selected foundation type due to its low cost, simple construction, and appropriateness for shallow water (Malhotra 2010). The design procedure for wind turbine monopiles still follows the semi-empirical p-y curve based on the low failure rate of in-service piles over many decades. The guidelines were established for long-flexible piles (embedded depth to diameter L/D ~ 34), for which the pile bending capacity is more critical than its rotation resistance. Consequently, the method has been revisited to evaluate its applicability to large-diameter monopiles. Experimental studies show that the stress-strain response for large-diameter monopiles is more flexible than that the American Petroleum Institute (API) calculation method because the soil resistance to the lateral movement of the pile is more developed with a mobilized friction angle (Dyson and Randolph 2001, Bienen *et al.* 2012, Choo and Kim 2016, Jeong *et al.* 2017). In addition, the large-diameter pile behaves as a rigid pile and the accumulated rotation (i.e., angular displacement) is more prevalent than the deflection on the pile head (Leblanc *et al.* 2010, Peng *et al.* 2011, Kuo *et al.* 2012, Arshad and O'Kelly 2016). Recently, a series of model tests under 1g conditions were conducted to investigate the pile-soil interaction during long-term lateral cyclic loading (Cuéllar *et al.* 2009, Shi *et al.* 2018). The experimental study showed that the pile subjected to cyclic lateral loading experienced a cone-shaped subsidence in the sand around the upper part of the pile and a densified truncated cone-shaped zone along the

*Corresponding author, Professor
E-mail: gyechun@kaist.edu
[a]Assistant Professor
E-mail: shchong@scnu.ac.kr
[b]Professor
E-mail: shingeo@ulsan.ac.kr

http://www.techno-press.org/?journal=gae&subpage=7
ISSN: 2005-307X (Print), 2092-6219 (Online)

pile shaft.

The long-term monopile response to repetitive loading is characterized by the evolution of displacements, pile rotation, and stress redistribution along the embedded pile. The effects of pile geometries and number of repetitive loadings on the soil response need to be better understood. This study explores the long-term soil response around offshore monopolies using the finite element method (FEM). A semi-empirical numerical approach is adopted to account for fundamental features of volumetric strain (terminal void ratio) and shear strain (shakedown and ratcheting), the strain accumulation rate, and stress obliquity. The parametric study includes pile diameter, embedded length, and moment arm distance from the surface. This manuscript starts with a review of fundamental features for long-term soil response. The numerical simulations under static and repetitive loads are presented next followed by an analysis of the results. In addition, further interpretation explains the propagation of shear localization that has been previously observed in the surrounding soil of monopile over a long period of time.

2. Fundamental features: Volumetric and shear strain

The analysis of the long-term soil response on geostructures requires characterizing the plastic strain accumulation, which depends on soil type and density, initial effective stress (static stress), cyclic stress amplitude and obliquity, and the number of cycles (Barksdale 1972, Brown 1974, Diyaljee and Raymond 1982, Stewart 1986, Kaggwa *et al.* 1991, Niemunis *et al.* 2005, Wichtmann *et al.* 2007, Karg *et al.* 2010, Wichtmann *et al.* 2010, Wichtmann *et al.* 2010). Strain accumulation approaches asymptotic conditions as the number of cycle increases.Volumetric strain and shearstrain are described by the asymptotic trend.

Volumetric strain: terminal void ratio. A soil specimen subjected to repetitive loading reaches a terminal void ratio and characteristic fabric (Narsilio and Santamarina 2008). While soils show contractive behavior, dilative soils strained significantly beyond their contraction-dilation transition point undergo disruption of interlocking and dilate as they evolve towards terminal density (Monismith *et al.* 1975, Luong 1980, Wichtmann *et al.* 2005). An experimental study under zero-lateral strain boundary condition exhibited a process-dependent compaction response towards the terminal void ratio (Chong and Santamarina 2016).

Shear strain: shakedown and ratcheting. Shear strain accumulation shows a wider range of asymptotic conditions. From previous studies focused on the analysis of soil fabric and measurement of energy losses, the following stages were classified (Koiter 1960, Barksdale 1972, Brown 1974, Sawczuk 1974, Monismith *et al.* 1975, Sharp and Booker 1984, García-Rojo and Herrmann 2005):

• Elastic shakedown: when cyclic loads cause a strain level below the elastic threshold strain, the soil recovers the original state upon unloading, and the dissipated energy per cycle remains constant thereafter; there is no creation or loss of interparticle contacts.

• Plastic shakedown: the strain level in each cycle exceeds the elastic threshold strain, the soil undergoes contact slippage and particle rearrangement in every cycle and energy dissipation involves frictional loss; yet, there is no accumulation of residual shear strain at the end of the cycle.

• Ratcheting: plastic shear strains continue accumulating in every cycle. While interparticle contacts change in every cycle, polar plots of contacts and contact forces analyzed at the end of every cycle converge towards constant asymptotic conditions after a large number of cycles.

3. Numerical methods

The numerical modeling of long-term geostructures needs to track the incremental plastic strain induced by each cycle and update the stress increment; yet the accumulation of physical deformation should be larger than the accumulation of numerical errors. To overcome implicit-based calculation, a semi-empirical explicit scheme was previously proposed that incorporates classical constitutive mode into the strain accumulations functions (Suiker and de Borst 2003, Niemunis *et al.* 2005, François *et al.* 2010, Kuo *et al.* 2012, Pasten *et al.* 2014). Some accumulation functions need the numerical cutoff criterion to stop accumulating plastic strain when the cyclic strain drops below the elastic threshold or when the void ratio reaches the terminal void ratio. The criterion at every incremental cycle should be checked with strains for all nodes, and thus requires higher computation cost during large number of cycles. This study adopts the semi-empirical explicit scheme, which satisfies the asymptotic conditions in the volumetric strain and shear strain. The algorithm is developed within the framework of FEM and consists of three steps, as summarized in Fig. 1.

3.1 Numerical algorithm

Step 1: Geostatic stress and first load cycle

Geostatic stress and initial static load are exerted on an offshore foundation using standard FEM and a mechanical constitutive model (stage O); the Modified Cam Clay model is utilized in this study. Then, the sequential loads are applied with maximum load (stage A), minimum load (stage B), and the initial static load (stage C); the initial load and cyclic amplitude are defined by the ultimate static load and safety factor. The stress and strain induced by the first cycle load reflect the combined effect of initial void ratio, initial effective stress (static stress), cyclic stress amplitude and obliquity. The calculated stress and strain are imposed at nodes and elements as the initial conditions of Step 2.

Step 2: Strain accumulation functions

As the number of load cycles increase, the volumetric strain asymptotically converges toward terminal density while the shear strain gradually reaches a constant value compatible with plastic shakedown state. In addition, the process-dependent strain accumulation requires the densification rate parameter α. The strain at the ith cycle are formulated as

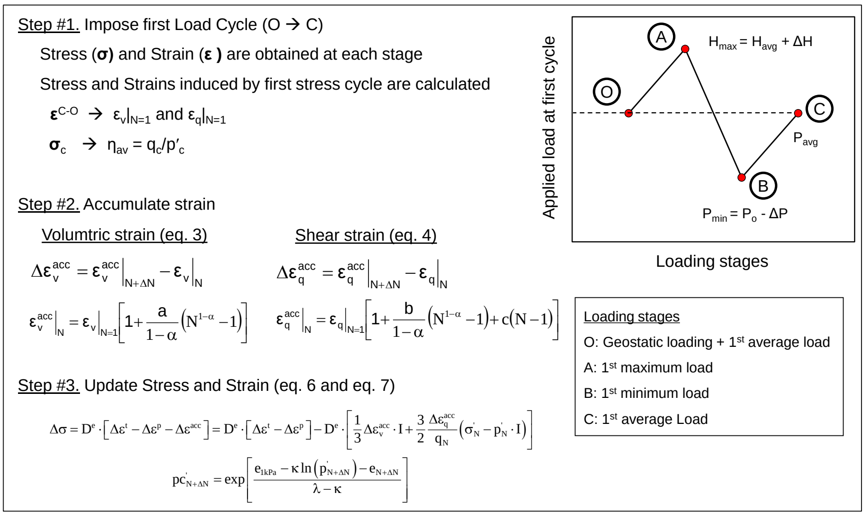

Fig. 1 Steps of numerical algorithm

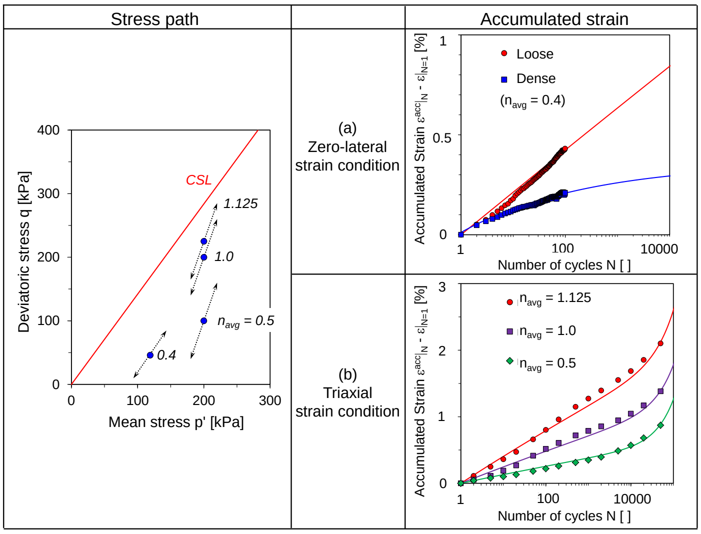

Fig. 2 Model calibration of the strain accumulation using repetitive loading test: (a) Zero-lateral strain condition – average static stress σ'_{avg} = 150 kPa, and vertical cyclic stress amplitude $\Delta\sigma'_v$ = 50 kPa (experimental data from Chong and Santamarina 2016); (b) Triaxial strain condition – average mean stress p'_{avg} = 200 kPa and cyclic stress amplitude Δq = 60 kPa (experimental data from Wichtmann 2005). The accumulated strain $\varepsilon_{acc} = [(\varepsilon_{axial})^2 + 2\cdot(\varepsilon_{radial})^2]^{0.5}$. Points are from experimental test and lines are from numerical simulation. The average stress obliquity $\eta_{avg} = q_{avg} / p_{avg}$

$$\varepsilon_v|_i = \varepsilon_v|_{N=1}\cdot\frac{a}{i^\alpha} \quad \text{where} \quad a(\eta_{avg}) = a_1(M-\eta_{avg})^2 + a_2 \tag{1}$$

$$\varepsilon_q|_i = \varepsilon_q|_{N=1}\cdot\left(\frac{b}{i^\alpha}+c\right) \quad \text{where} \quad b(\eta_{avg}) = -b_1(\eta_{avg}) + b_2 \quad \text{and} \quad c(\eta_{avg}) = c_1(\eta_{avg}) \tag{2}$$

The parameters a, b, and c are constitutive parameters that reflect the effect of the average stress obliquity n_{avg} (=q_{avg}/p_{avg}) and critical state frictional state M. In particular, the parameter c > 0 indicates the soil reaches ratcheting for i → ∞. By integrating equations 1 and 2 from i =1 to N, the accumulated strains in a given load cycle N can be established as

$$\varepsilon_v^{acc}\Big|_N = \varepsilon_v|_{N=1} + \varepsilon_v|_{N=1}\cdot\frac{a}{1-\alpha}\left(N^{1-\alpha}-1\right) \tag{3}$$

$$\varepsilon_q^{acc}\Big|_N = \varepsilon_q|_{N=1} + \varepsilon_q|_{N=1}\cdot\left[\frac{b}{1-\alpha}\left(N^{1-\alpha}-1\right)+c(N-1)\right] \tag{4}$$

The volumetric strain accumulation with average stress obliquity (n_{avg} = M) close to critical state becomes zero. Thus, the terminal volumetric strain can be formulated from Eq. (3) as i → ∞

$$\varepsilon_v^{acc}\Big|_{N=\infty} = \varepsilon_v|_{N=1}\cdot\left(1-\frac{a}{1-\alpha}\right) \tag{5}$$

These polynomial-type strain accumulation functions

Table 1 Model parameters used in this study: (a) Modified Cam Clay parameters and (b) Strain accumulation functions. The loose sand properties for Ko condition are used to simulate the long-term monopile foundation in section 4.2

(a) MCC Parameters	Symbol	Value
Unit weight [kN/m3]	γ	18.0
Isotropic compression [ ]	λ	0.01
Isotropic recompression [ ]	κ	0.001
Drained Poisson's ratio [ ]	υ	0.3
MCC strength (for Axial Compression)	M	1.42
Friction angle [o]	ϕ'	35
Void ratio at 1kPa [ ]	e1kPa	0.785
Coefficient of earth pressure at rest [ ]	Ko	0.58

(b) Empirical strain accumulation functions

	Stress obliquity	Accumulated strain rate	Accumulated volumetric strain $\Delta\varepsilon_v^{acc}\vert N$		Accumulated shear strain $\Delta\varepsilon_q^{acc}\vert N$		
	ηavg	α	a1	a2	b1	b2	c1
Triaxial condition	0.5	1.02	0.5	1.0	-0.15	0.8	$8\cdot10^{-5}$
	1	1.02	0.5	1.0	-0.15	0.65	$5\cdot10^{-5}$
	1.125	1.02	0.5	1.0	-0.15	0.62	$3\cdot10^{-5}$
K_o condition	0.4 (Loose)	1.01	0.31	0.4	-0.56	0.4	0
	0.4 (Dense)	1.18	0.48	0.4	-0.71	0.4	0

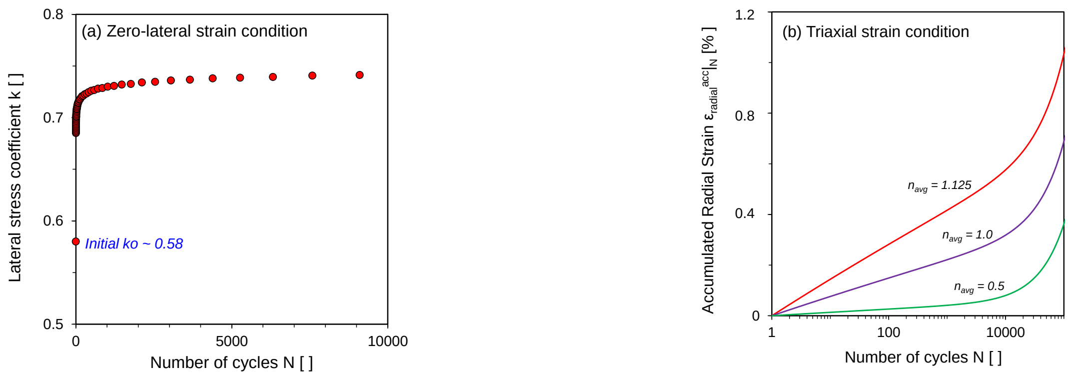

Fig. 3 Element tests of strain accumulation: (a) Zero-lateral strain test - Evolution of lateral stress coefficient and (b) Triaxial test - Cumulative radial strain.

satisfy the fundamental features of volumetric strain and shear strain, the strain accumulation rate, and stress obliquity.

Step 3: Incremental stress and strain during ΔN cycle

The stress increment $\Delta\sigma$ during ΔN cycle is updated with the accumulated strain vector defined by plasticity

$$\Delta\sigma = D^e \cdot \left[\Delta\varepsilon^t - \Delta\varepsilon^p - \Delta\varepsilon^{acc}\right] = D^e \cdot \left[\Delta\varepsilon^t - \Delta\varepsilon^p\right] - D^e \cdot \left[\frac{1}{3}\Delta\varepsilon_v^{acc} \cdot I + \frac{3}{2}\frac{\Delta\varepsilon_q^{acc}}{q_N}\left(\sigma'_N - p'_N \cdot I\right)\right] \quad (6)$$

where D^e is the elastic stiffness matrix [6×6], $\Delta\varepsilon^t$ and $\Delta\varepsilon^p$ are total and plastic strain increments [6×1], I is identify vector [6×1], p'_N and q_N are mean and deviatoric stress components of the stress state from the previous cycle N. The stress increment updated by the accumulated strains caused unbalanced forces in the system. The unbalanced forces are equilibrated in subsequent iterations. The preconsolidation pressure pc' that defines the size of the yield surface is calculated with the updated void ratio and effective mean stress

$$pc'_{N+\Delta N} = \exp\left[\frac{e_{1kPa} - \kappa \ln\left(p'_{N+\Delta N}\right) - e_{N+\Delta N}}{\lambda - \kappa}\right] \quad (7)$$

where e_{1kPa} is the void ratio at 1kPa, λ is the isotropic compression, and κ is the isotropic recompression. The load cycle increment ΔN significantly affects numerical stabilities. In particular, the early cycles ($N < 100$) produces the most pronounced displacements. Thus, the load cycle was increased with the exponential function $N = 1.2^m$, where m is integer number increment from 0.

3.2 Model calibration

The numerical algorithm was implemented using the UMAT subroutine in ABAQUS 6.14. The model calibration is performed with different strain boundary conditions and stress obliquity. The constitutive parameters (a, b, c) are defined by formal inversion (note that the strains induced by the first loading and the model parameters remain constant during numerical simulation). Fig. 2 shows the comparison between experimental data from previous studies (Wichtmann 2005, Chong and Santamarina 2016) and the numerical simulations from this study for accumulated strain. For the zero-lateral strain condition, the model matches well with the adopted densification rate parameter. The calibrated model parameters are summarized in Table 1. The terminal volumetric strain can be computed with the calibrated constitutive parameters by using equation 5. This analysis shows that a soil element with the densification factor α = 1.14 and the average stress obliquity η_{avg} = 0.4 reaches a terminal volumetric strain $\varepsilon_v|_{N\to\infty}$ = 0.015 if $\varepsilon_v|_{N\to\infty}$ = 0.001. Also, the model tested with the triaxial strain conditions predicts the measured data with a different rate of strain accumulation under different stress obliquity. While limited data is used to adjust the numerical model, the comparisons confirm that the strain function with the relaxation of these parameters can be suitable for tracking the incremental plastic strains induced by different strain boundary conditions and stress obliquities.

3.3 Physical validation

Fig. 3(a) shows the evolution of the horizontal to vertical stress ratio k = σ'h/σ'v under a zero-lateral strain boundary condition. The stress ratio largely increases during the first few cycles and converges towards the asymptote for a large number of cycles. Similar results are observed in experimental tests under a zero-lateral strain condition (Finn 1981, Bouckovalas *et al.* 1984, Sawicki 1994, Sawicki and Swidzinski 1995). Fig. 3(b) shows the calculated cumulative radial strain with the number of load cycles under the triaxial strain condition. Higher average stress obliquity η_{avg} produces more cumulative strain, as observed in previous studies (Chang and Whitman 1988, Wichtmann *et al.* 2010).

4. Simulation of monopile foundation

A monopile foundation is simulated by imposing a static load followed by a repetitive load due to the lack of the load history. The initial static load and load amplitude are defined by the ultimate static load which varies with pile geometries (diameter D, and embedded length L, and moment arm distance from the surface h). Thus, the ultimate lateral load is numerically investigated under static load, followed by a monopile response to the repetitive loads.

4.1 Ultimate lateral resistance under static load

The study of piles has been advanced in the context of transmission lines, power stations, heavy buildings, and highway structures. In many cases, lateral loads govern the design of piles. The soil resistance to the lateral movement of the pile is characterized by the distribution of lateral stress in front of the pile and the side shear friction. The stress distribution around the pile subjected to lateral load is affected by pile shape (Smith 1987). Several methods have been proposed to calculate the ultimate lateral resistance of free-headed laterally-loaded rigid piles based on a simplified horizontal stress distribution along the pile length (Broms 1964, Reese *et al.* 1974, Meyerhof *et al.* 1981, Meyerhof *et al.* 1988, Prasad and Chari 1999, Zhang *et al.* 2005). The ultimate lateral load can be obtained from numerical integration of the net horizontal stress by subtracting the passive stress from the active one. The numerically computed load is compared with two empirical methods. The Broms method assumes that only passive earth pressure linearly increases along the pile and the active pressure is ignored. By considering the influence of pile shape for a 2D numerical analysis, the ultimate lateral load can be rewritten as (Broms 1964)

$$H_{ult-static} = 0.56\frac{\gamma\sqrt{D}\cdot K_p{}^2}{h+L} \tag{8}$$

where h is the moment arm distance from the ground surface, L is the embedded pile length, D is the pile diameter, and Kp is the passive earth pressure. Meanwhile, the method by Zhang *et al.* includes the pile-soil interface resistance and the rotation distance from the ground surface and properly predicts the lateral resistance obtained from both flexible and rigid model piles (Zhang *et al.* 2005). The ultimate lateral load (Hult-static) can be rewritten as

$$H_{ult-static} = 0.34\gamma\sqrt{D}\cdot\left(K_p{}^2 + 2K\tan\delta\right)\cdot\left(2.7a^2 - 1.7La\right) \tag{9a}$$

$$a = \frac{-\left(0.6L + 2.7h\right) + \left(5.3L^2 + 7.3h^2 + 10.5hL\right)^{0.5}}{2.2} \tag{9b}$$

where K is the lateral earth pressure coefficient, a is the rotation distance calculated by equation 9b, and δ is the interfacial friction angle between the pile and soil. The K value is defined by the pile type and construction method and its typical range for normally consolidated sediment varies between 0.3 and 1.0 (Kulhawy 1991). K (~ 0.58) is selected for this study, equal to the initial Ko value. The interfacial friction angle is related to numerical stability. A pile subjected to horizontal cyclic loading compresses and expands soil elements, and thus the relaxation at the interface between the soil and pile leads to numerical instability (Tuladhar *et al.* 2008). Contact elements based on Coulomb friction theory are employed to improve contact interaction between the pile and soil elements. The value of δ/ϕ' varies between 0 and 1, depending on the surface roughness, mean particle size of the sand, and the method of installation (Tiwari and Al-Adhadh 2014). As in the case of a smooth steel pipe pile, δ is taken as two-thirds of the friction angle of the soil (δ=2/3ϕ'). In fact, the installation of a driven pile foundation inherently disturbs the soil around the pile; however, the disturbance effect is not considered in the numerical modeling because the plastic zone induced by horizontal repetitive loading is much larger than the installation disturbance (Achmus *et al.* 2009).

The monopile response to static loading is simulated under a plane strain boundary condition with four-node full

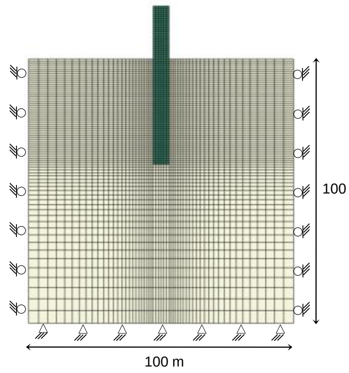

Fig. 4 Geometry and boundary conditions used in this study

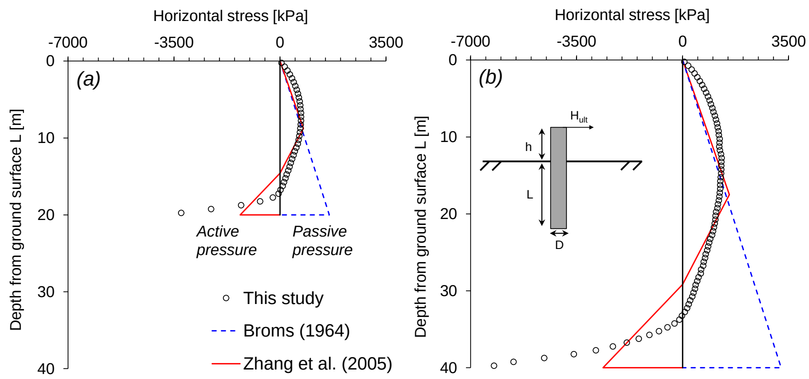

	$H_{ult\text{-}static}$ [MN]	
	(a)	(b)
Broms (1964)	7.1	28.3
In this study	3.2	11.6
Zhang et al. (2005)	2.1	8.3

Fig. 5 Horizontal stress distribution along the embedded length of the pile when a static load is laterally applied to the pilehead. (a) L/D = 6.7 and (b) L/D = 13.3. The pile diameter D is 3m and the relative length of pile is fixed as h/L = 0.5. Horizontal stress is obtained by subtracting the passive stress from the active one and continuous lines are estimated using Eqs. (8) and (9).

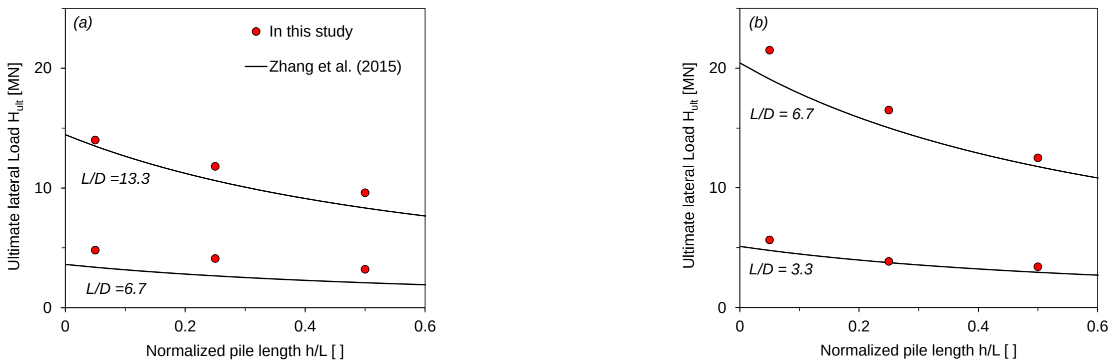

Fig. 6 Effect of pile geometries on ultimate lateral resistance under static loads applied at the top of the pile. (a) D = 3 m; (b) D = 6 m. Continuous lines in (a) and (b) are obtained from equation (2). The stress transmitted through pile is concentrated at the node shared by pile element and soil element and a perfectly embedded pile (h = 0 m) is limited by numerical instability

integration elements. As shown in Fig. 4, the domain size is 100 m high and 100 m wide. Lateral boundaries are located far from the monopile to minimize boundary effects on surface settlements; vertical displacement is allowed on side boundaries, the bottom boundary is pinned, and the top surface is free. The pile is modeled as a linearly elastic material: a pile made of concrete with unit weight $\gamma con = 25$ kN/m^3, Young's modulus E_{con} = 200 GPa, and Poisson's

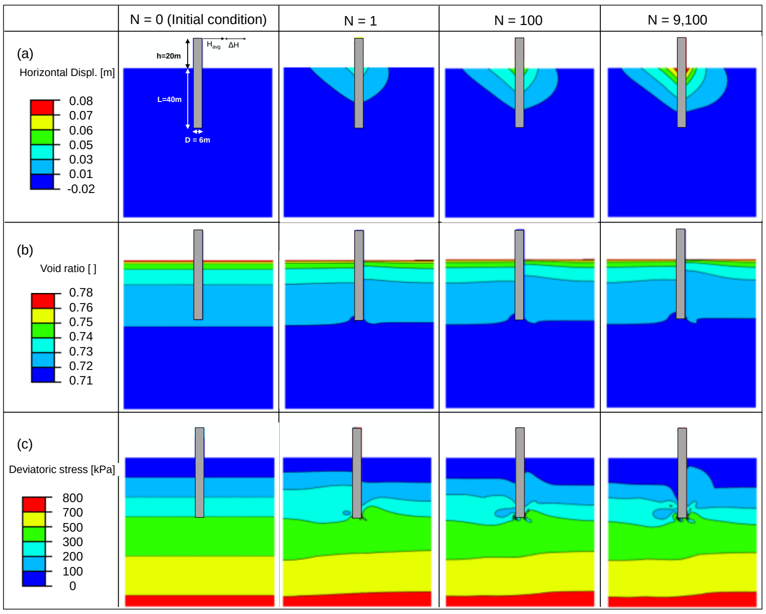

Fig. 7 Monopile foundation response to horizontal repetitive load for different cycles: (a) Accumulation of horizonta displacement; Distribution of (b) void ratio and (c) deviatoric stress.

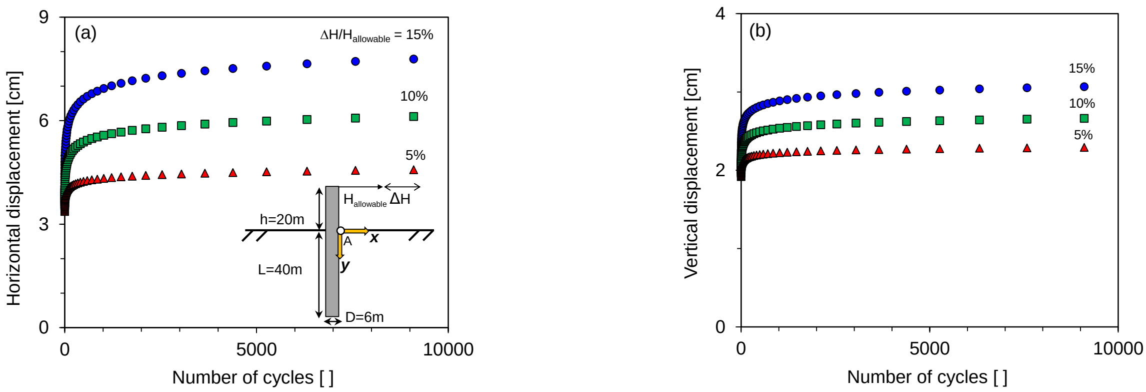

Fig. 8 Effect of horizontal load amplitude on the displacement evolution of a pile foundation: (a) Horizontal displacement; (b) Vertical displacement. The displacements are measured at the ground surface (Point A) and their signs follow the coordinates. The horizontal load amplitudes ΔH are defined by 5%, 10%, and 15% of Hallowable ~ 2.1 MN (FS = Hult / Havg ~ 6).

ratio υ_{con} = 0.3. A parametric study is conducted to explore the effect of pile geometries on the ultimate static load resistance. Note that the vertical load has little effect on the lateral load-carrying capacity of the monopile (Ahmed and Hawlader 2016). Numerically computed load resistance is obtained from formal load control that increases the applied horizontal load on the pile head until numerical instability occurs. The applied load is limited by mesh distortion (the determinant of the Jacobian matrix approaches zero and the stiffness integral cannot be solved). For example, a perfectly embedded pile (h=0m) fails to reach the ultimate lateral resistance because the stress transmitted through the pile is concentrated at the node shared by pile-and soil-elements, and thus the neighboring elements are highly distorted.

Pile rigidity has a pronounced effect on the pile-soil response. A free-head rigid pile under lateral load shows linear displacement along the embedded pile and develops the movement even at the pile end. For a flexible pile, significant displacement occurs on the upper part of the pile. Previous studies proposed rigidity parameters involving pile and soil stiffness to characterize a rigid or flexible pile (Broms 1964, Poulos and Davis 1980, Randolph 1981, Briaud *et al.* 1984). Also, the relative pile geometric ratio (length to diameter, L/D) can identify pile response; L/D > 10 (longer pile embedded length) behaves as flexible pile, otherwise it behaves as a rigid pile. This study adopts the pile geometric ratio for simplicity. (Peng *et al.* 2011, Arshad and O'Kelly 2016).

Fig. 5 presents the horizontal stress distribution along the pile. When the static load is laterally applied to the node at the pile head, passive pressures are developed at the front face above the rotation point of the pile and active pressures are formed at the corresponding back face. The trend of passive stress follows an elliptical shape, yet active stress linearly increases from the rotation point to the pile end. The numerically computed horizontal stress trends are compared with two empirical equations. While Broms

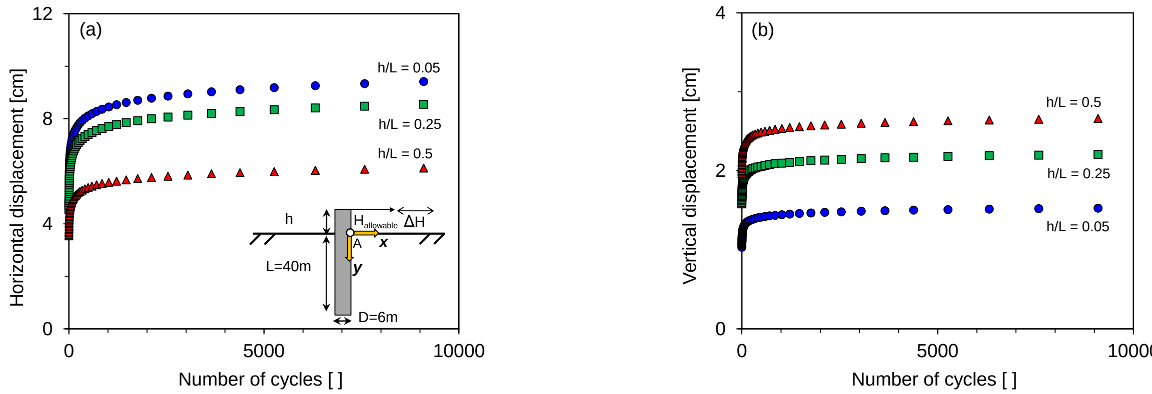

Fig. 9 Effect of moment arm distance on the displacement evolution of a pile foundation: (a) Horizontal displacement and (b) Vertical displacement. The displacements are measured at the ground surface (Point A). The average and cyclic loads are Hallowable = Hult / 6 and ΔH = 0.10·Hallowable for ultimate lateral resistance Hult defined by static load shown in Fig. 6

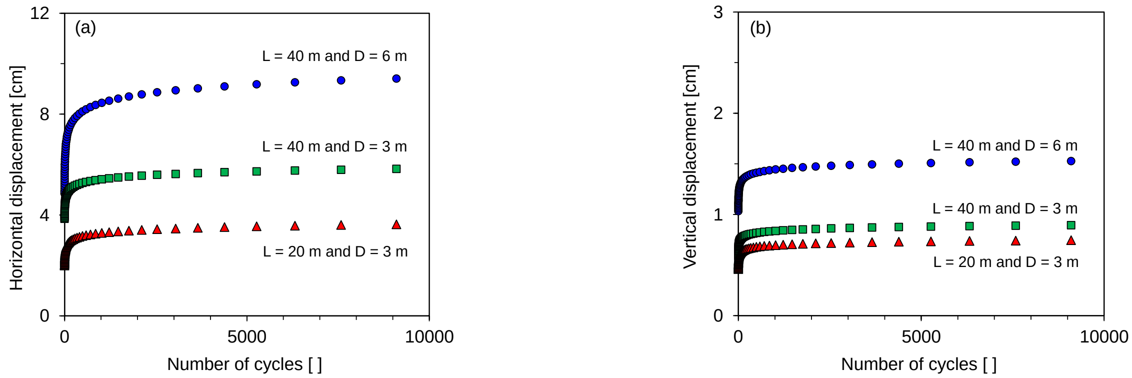

Fig. 10 Effect of pile geometries (embedded pile depth L and diameter D) on the displacement evolution of a pile foundation subjected to repetitive loading: (a) Horizontal displacement and (b) Vertical displacement. The relative length of the pile is fixed as h/L = 0.05. Note that the horizontal load amplitude ratio taken as 10% in all cases is defined by the ultimate lateral load corresponding to its pile geometry (Fig. 6)

method, which disregards the horizontal stress on the active side, overestimates the ultimate lateral resistance, the Zhang method captures the shape of horizontal stress. In addition, the rotation point is approximately located at around 0.75L in both cases. The numerically observed rotation point was approximately 0.78L (for h ≈ 0) and decreased with longer moment arm. The typical range is 0.7L ~ 0.78L for the monopile foundation (Ahmed and Hawlader 2016). Different pile geometries are simulated and compared with the Zhang method, as shown in Fig. 6. A longer pile embedded in soil elements (higher L/D) enhances the ultimate lateral resistance due to a higher overturning moment, yet the ultimate load is decreased with higher eccentricity (longer h). The comparison shows that the numerical analysis causes slightly higher ultimate horizontal load than the Zhang method in all cases.

4.2 Monopile foundation response to repetitive load

A monopile foundation on sand is simulated by imposing a static load ($H_{allowable}$) followed by repetitive lateral load (±ΔH). The numerically predicted lateral resistance is H_{ult} = 12.6 MN for L/D = 6.7 and h/L = 0.5 (Fig. 6(b)). Thus, average static load $H_{allowable}$ = 2.1 MN (factor of safety FS = 6) and cyclic load amplitude ΔH = 0.32MN (0.15·$H_{allowable}$) are applied on the node at pile top.

Fig. 7 presents the stress and strain fields according to the number of cycles. The horizontal repetitive load produces horizontal displacements (Fig. 7(a)). The plastic displacement initiates in soil elements located on the ground surface, yet propagates along the soil elements up to the neighboring toe of the pile. The repetitive loads cause additional horizontal displacement of 4 cm after N = 9,100. Correspondingly, the void ratio field shows a "soil densification effect" (Fig. 7(b)). The void ratio gradually decreases at the passive side and the pile end. A previous experimental study observed that the sand surrounding the pile subjected to cyclic horizontal load on the pile head undergoes densification and grain migration. It reveals the clear presence of two distinct sand domains due to convective granular flow near the pile (Cuéllar *et al.* 2009). Further interpretation is provided in the Discussion section of this paper. The deviatoric stress field shows either strength-hardening or- softening, depending on the pile side (Fig. 7(c)). The repetitive load increases the shear resistance following the loading direction while the opposite side undergoes repetitive softening that propagates toward the pile end.

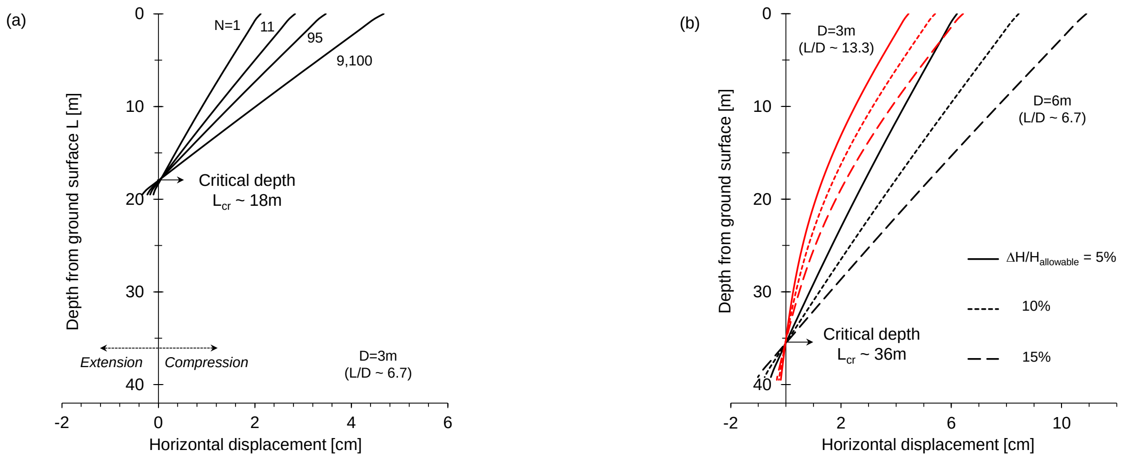

Fig. 11 Evolution of horizontal displacement along a monopile foundation: (a) Number of cycles (D = 3 m) and (b) Horizontal load amplitudes (N = 1,021). The displacements are measured at nodes along the pile. The relative length of pile is h/L = 0.05

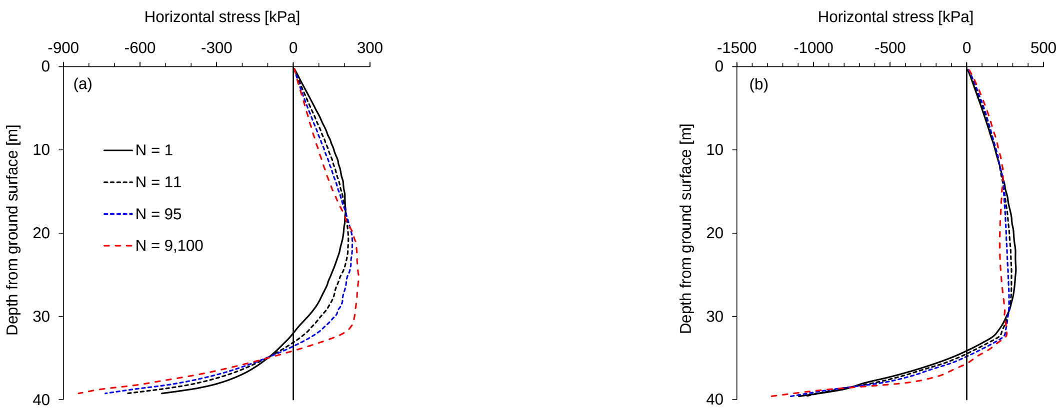

Fig. 12 Change in horizontal stress along a monopile foundation subjected to repetitive lateral loads: Redistribution of lateral stress with (a) D = 3 m (flexible pile) and (b) D = 6 m (rigid pile) for load cycles N=1, 11, 95, and 9,100. The relative length of pile is h/L = 0.05. Lateral stress is obtained by subtracting the active stress from the passive stress on the pile

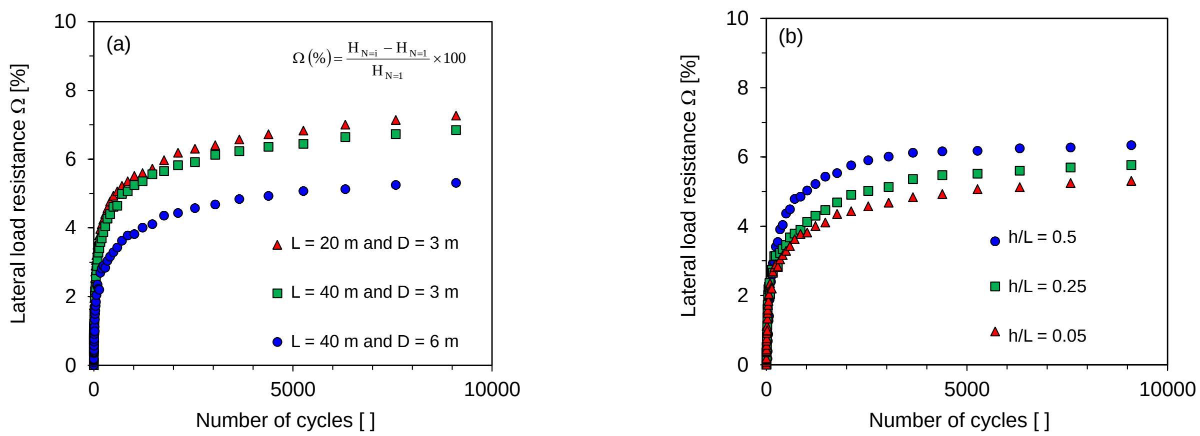

Fig. 13 Evolution of lateral load resistance: (a) Pile geometry (h/L = 0.05) and (b) Moment arm distance (L = 40 m and D = 6 m). Lateral load resistance at end of each cycle is calculated from numerical integration of lateral stress shown in Fig. 11

Repetitive load amplitude, which plays a crucial role in characterizing long-term pile response, has a pronounced effect on the accumulation of vertical and horizontal displacements (Fig. 8). The horizontal load amplitude is defined by the ultimate horizontal load computed from a static simulation (Fig. 6) and safety factor (FS = 6). While both displacements increase proportionally to the repetitive load amplitude, horizontal displacement is larger than vertical displacement. Most displacements occur during early cycles (N < 100), yet their accumulation rate is decreased for a large number of cycles. The asymptotic displacement increases with higher horizontal load amplitude. As anticipated, cumulative displacements become more pronounced as FS decreases.

An offshore monopile undergoes the eccentric load induced by wind and waves that act on the upper part of the pile. The effects of eccentric loads on the displacement of the monopile are examined as shown in Fig. 9. The simulation presents that a shorter eccentric ratio (h/L) produces larger horizontal displacement at the ground surface, yet the vertical displacement show contrary trend. This is because the repetitive horizontal load with larger moment arm (i.e., longer h) mostly contributes to the vertical response.

Fig. 10 shows the effect of pile geometry on the evolution of displacement. When the repetitive horizontal load corresponding to each pile geometry ratio (L/D) is exerted on the pile head, larger diameter (at the same embedded depth) or longer embedded pile depth (at the same diameter) piles produces larger displacements. It should be noted that if the same magnitudes of horizontal load are applied to different pile geometry, the longer h/L or lower L/D pile would produce more displacement.

Fig. 11 presents the evolution of horizontal displacements along the pile. After the first cycle, the pile experiences a displacement transition from compression to extension. In Fig. 11(a), the critical depth (distance from ground surface to the transition point) remains constant after the number of cycles, while the horizontal displacement gradually evolves from the zero displacement point. The critical depth is approximately located at around 0.9L regardless of embedded pile depth; the longer moment arm distance h slightly reduces the critical depth for both rigid and flexible piles (from 36 m to 33 m – not presented here). In fact, previous simulations observed that the embedded pile depth has little influence on the critical depth (Achmus *et al.* 2009, Kuo *et al.* 2012). Higher horizontal load amplitude increases the displacement along pile (Fig. 11(b)). The trends of horizontal displacement are significantly affected by relative pile geometry ratio. A low L/D ratio (L/D ~ 6.7) exhibits a rigid pile response where the displacement linearly increases from the embedded pile depth. Meanwhile, a flexible pile (L/D ~ 13.3) shows a nonlinear pattern of displacement where incremental rate of displacement largely increases toward the ground surface.

The variation in lateral stress along the pile is explored as shown in Fig. 12. The initial regime of active pressure decreases and its magnitude increases around the pile end. However, the pile rigidity results in a distinct pattern on the passive side. For the flexible pile, horizontal stress decreases until the upper part of the pile, yet increases from the middle part of the pile (Fig. 12(a)). The rigid pile (larger diameter) shows that a local reduction of the horizontal stress takes place around the middle of the pile (Fig. 12(b)).

The lateral load resistance in each cycle is calculated from numerical integration of the net lateral stress by subtracting the active stress from the passive stress. The lateral load resistance is evaluated in terms of the dimensionless ratio

$$\Omega\,(\%) = \frac{H_{N=i} - H_{N=1}}{H_{N=1}} \times 100 \tag{10}$$

Fig. 13 shows the evolution of the lateral load resistance with the number of cycles. In all cases, the repetitive lateral load enhances the lateral load resistance followed by soil densification around the pile.

5. Discussion

5.1 Propagation of shear localization around pile

An insightful investigation into the long-term pile response was conducted by observing the particle movements as a function of the number of cycles (Cuéllar *et al.* 2009). It was revealed that the sediment surrounding the pile subjected to cyclic horizontal load experiences coupled densification and granular convection related to particle rearrangement and constant sliding as the main mechanisms for plastic deformation; as the pile moves back and forth, the stress relaxation at the pile-soil interface enables the sand grains adjacent to the pile-head to move downwards along the interface. Once the grains are densely packed up to the critical depth, they could not move further down. The rotation frustrations among the grains are overcome with frictional slippage at contact and the migrating grains would move forward pushed by the following grains. While they move toward the ground surface, the convective granular flow occurs within the pile-head vicinity. The shear band formed by the coupled densification and granular convection is captured with the numerical continuum model used in this study (Fig. 14). The numerically observed gradient of shear stress at the end of cycle shows the propagation of shear localization from the pile tip to the ground surface, which is very similar to the shear band marked by the mixture of colored particles. In addition, the progressive pile movement induced by the horizontal repetitive loads eventually changes the passive failure line developed from the pile tip. The failure line formed by the tangent line to the trajectory is greater than the passive failure line ($=45 - \phi'/2$) because the repetitive loads improves the passive resistance defined by the static load.

5.2. Uncertainty of friction angle

Friction angle plays a controlling role in accumulating the soil deformations around the pile. For the static load, the mobilized angle of internal friction and dilation angle is characterized by the relative density, confining pressure, and plastic shear strain. In particular, the friction anisotropy is observed in triaxial axial extension AE and compression cases AC for normally consolidated clays (Mayne and Holtz 1985). The repetitive loads increase the interaction between the pile and the surrounding soils and progressively change the interfacial friction angle. Furthermore, the Modified Cam Clay model used in this study fails to not only predict the observed softening and dilatancy of dense sands, but also recognize the mobilized friction angle during the repetitive loads. Indeed, the soils around the monopile experience a different stress path and accumulated strain levels, and thus the selection of friction angle involves large uncertainty.

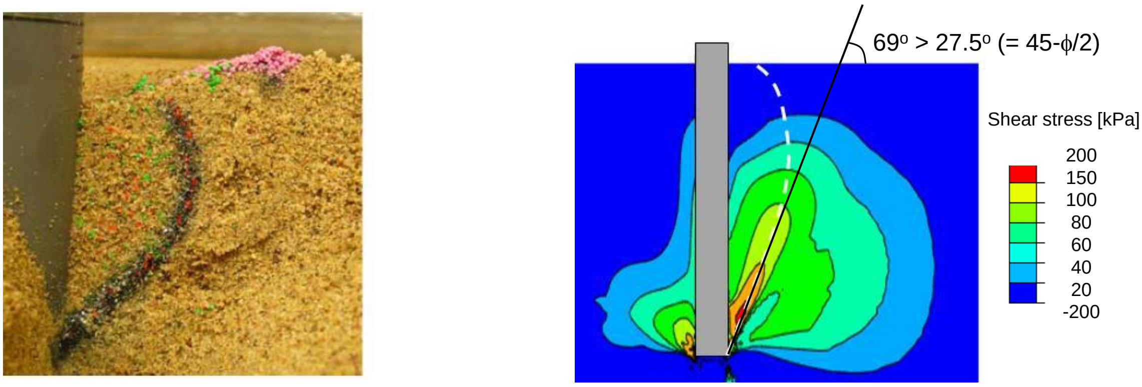

(a) Experimental test (Cuéllar *et al.*, 2009) (b) Numerical simulation (N = 9,100)

Fig. 14 Comparison between (a) experimentally-observed and (b) numerically-observed shear localization. In (b), the dotted line is the trajectory along the gradients of shear stress and the continuous line is tangent to the trajectory

6. Conclusions

This study analyzes a monopile foundation subjected to repetitive loads. A semi-empirical numerical scheme that consists of two parts is used (1) to extract stress and strains at the first cycle using the Modified Cam Clay model and (2) to track the progressive accumulation of plastic deformation during repetitive loading using an empirical accumulation function. In particular, the strain function contains fundamental features to capture the long-term soil behavior: volumetric strain (terminal void ratio) and shear strain (shakedown and ratcheting), the strain accumulation rate, and stress obliquity. A model is calibrated under different strain boundary conditions by relaxing four model parameters.

Numerical simulations show the accumulation of vertical and horizontal displacements and stress redistribution with the number of horizontal load cycles. Higher horizontal load amplitude accumulates larger displacements. The relative pile geometry (embedded pile length to diameter ratio L/D) has a pronounced effect on the trends of the horizontal displacement profile. The low L/D ratio (L/D ~ 6.7) exhibits a rigid pile response where the displacement linearly increases from the embedded pile depth. Meanwhile, the flexible pile (L/D ~ 13.3) shows a nonlinear pattern of displacement where the incremental rate of displacement largely increases toward the ground surface. The pile rigidity causes a distinct pattern on the passive side formed along the loading direction. For the flexible pile, horizontal stress decreases up to the upper part of the pile, yet increases from the middle part of the pile. The rigid pile (larger diameter) shows that a local reduction of the horizontal stress occurs around the middle of the pile. The numerically computed lateral load resistance increases with the number of load cycles due to the soil densification around the pile. Further analysis reveals that the convective granular flow is drawn by the gradient of shear stress at the end of the cycle.

Acknowledgments

This research was supported by the National Research Foundation of Korea (NRF) grant funded by the Korea government (MSIT) (No. 2017R1A5A1014883).

References

ABAQUS 6.14 [Computer software], Dassault Systèmes, Providence, Rhode Island, U.S.A.

Achmus, M., Kuo, Y.S. and Abdel-Rahman, K. (2009), "Behavior of monopile foundations under cyclic lateral load", *Comput. Geotech.*, **36**(5), 725-735. https://doi.org/10.1016/j.compgeo.2008.12.003.

Ahmed, S.S. and Hawlader, B. (2016), "Numerical analysis of large-diameter monopiles in dense sand supporting offshore wind turbine", *Int. J. Geomech.*, **16**(5), 04016018. https://doi.org/10.1061/(ASCE)GM.1943-5622.0000633.

API (2000), "Recommended practice for planning, designing and constructing fixed offshore platforms: Working stress design", American Petroleum Institute.

Arshad, M. and O'Kelly, B.C. (2016), "Model studies on monopile behavior under long-term repeated lateral loading", *Int. J. Geomech.*, **17**(1), 04016040. https://doi.org/10.1061/(ASCE)GM.1943-5622.0000679.

Barksdale, R.D. (1972), "Laboratory evaluation of rutting in basecourse materials", *Proceedings of the 3rd International Conference on Structural Design of Asphalt Pavements*, London, U.K., September.

Bienen, B., Dührkop, J., Grabe, J., Randolph, M. and White, D. (2012), "Response of piles with wings to monotonic and cyclic lateral loading in sand", *J. Geotech. Geoenviron. Eng.*, **138**(3), 364-375. https://doi.org/10.1061/(ASCE)GT.1943-5606.0000592.

Bouckovalas, G., Whitman, R. and Marr, W. (1984), "Permanent displacement of sand with cyclic loading", *J. Geotech. Eng.*, **110**(11), 1606-1623. https://doi.org/10.1061/(ASCE)0733-9410(1984)110:11(1606).

Briaud, J.L., Smith, T.O. and Meyer, B.J. (1984), "Using the pressuremeter curve to design laterally loaded piles", *Proceeding of the 15th Annual Offshore Technology Conference*, Houston, Texas, U.S.A., January.

Broms, B.B. (1964), "Lateral resistance of piles in cohesive soils", *J. Soil Mech. Found. Div.*, **90**(3), 123-158.

Brown, S.F. (1974), "Repeated load testing of a granular material", *J. Geotech. Eng. Div.*, **100**(7), 825-841.

Chang, C. and Whitman, R. (1988), "Drained permanent deformation of sand due to cyclic loading", *J. Geotech. Eng.*, **114**(10), 1164-1180.

https://doi.org/10.1061/(ASCE)0733-9410(1988)114:10(1164).

Chong, S.H. and Santamarina, J.C. (2016), "Sands subjected to repetitive vertical loading under zero lateral strain: Accumulation models, terminal densities, and settlement", *Can. Geotech. J.*, **53**(12), 2039-2046. https://doi.org/10.1139/cgj-2016-0032.

Choo, Y.W. and Kim, D. (2016), "Experimental development of the p-y relationship for large-diameter offshore monopiles in sands: Centrifuge tests", *J. Geotech. Geoenviron. Eng.*, **142**(1), 04015058. https://doi.org/10.1061/(ASCE)GT.1943-5606.0001373.

Cuéllar, P., Baeßler, M. and Rücker, W. (2009), "Ratcheting convective cells of sand grains around offshore piles under cyclic lateral loads", *Granul. Matter*, **11**(6), 379-390. https://doi.org/10.1007/s10035-009-0153-3.

Diyaljee, V.A. and Raymond, G.P. (1982), "Repetitive load deformation of cohesionless soil", *J. Geotech. Eng. Div.*, **108**(10), 1215-1229.

Dyson, G.J. and Randolph, M.F. (2001), "Monotonic lateral loading of piles in calcareous sand", *J. Geotech. Geoenviron. Eng.*, **127**(4), 346-352. https://doi.org/10.1061/(ASCE)1090-0241(2001)127:4(346).

Finn, W.D.L. (1981), "Liquefaction potential: Developments since 1976", *Proceedings of the International Conference on Recent Advances in Geotechnical Earthquake Engineering and Soil Dynamics*, St. Louis, Missouri, U.S.A., April-May.

François, S., Karg, C., Haegeman, W. and Degrande, G. (2010), "A numerical model for foundation settlements due to deformation accumulation in granular soils under repeated small amplitude dynamic loading", *Int. J. Numer. Anal. Meth. Geomech.*, **34**(3), 273-296. https://doi.org/10.1002/nag.807.

García-Rojo, R. and Herrmann, H.J. (2005), "Shakedown of unbound granular material", *Granul. Matter*, **7**(2-3), 109-118. https://doi.org/10.1007/s10035-004-0186-6.

Jeong, S., Park, J., Ko, J. and Kim, B. (2017), "Analysis of soil resistance on drilled shafts using proposed cyclic p-y curves in weathered soil", *Geomech. Eng.*, **12**(3), 505-522. https://doi.org/10.12989/gae.2017.12.3.505.

Kaggwa, W., Booker, J. and Carter, J. (1991), "Residual strains in calcareous sand due to irregular cyclic loading", *J. Geotech. Eng.*, **117**(2), 201-218. https://doi.org/10.1061/(ASCE)0733-9410(1991)117:2(201).

Karg, C., François, S., Haegeman, W. and Degrande, G. (2010), "Elasto-plastic long-term behavior of granular soils: Modelling and experimental validation", *Soil Dyn. Earthq. Eng.*, **30**(8), 635-646. https://doi.org/10.1016/j.soildyn.2010.02.006.

Koiter, W.T. (1960), *General Theorems for Elastic-Plastic Solids*, Amsterdam, The Netherlands.

Kulhawy, F.H. (1991), *Drilled Shaft Foundations*, in *Foundation Engineering Handbook*, Springer, Boston, Massachusetts, U.S.A., 537-552.

Kuo, Y.S., Achmus, M. and Abdel-Rahman, K. (2012), "Minimum embedded length of cyclic horizontally loaded monopiles", *J. Geotech. Geoenviron. Eng.*, **138**(3), 357-363. https://doi.org/10.1061/(ASCE)GT.1943-5606.0000602.

Leblanc, C., Houlsby, G.T. and Byrne, B.W. (2010), "Response of stiff piles in sand to long-term cyclic lateral loading", *Geotechnique*, **60**(2), 79-90. https://doi.org/10.1680/geot.7.00196.

Luong, M.P. (1980), "Stress-strain aspects of cohesionless soils under cyclic and transient loading", *Proceeding of the International Symposium on Soils under cyclic and transient loading*, Swansea, Wales, U.K., January.

Malhotra, S. (2010), "Design and construction considerations for offshore wind turbine foundations in North America", *Proceedings of the GeoFlorida 2010: Advances in Analysis, Modeling & Design*, West Palm Beach, Florida, February.

Mayne, P.W. and Holtz, R.D. (1985), "Effect of principal stress rotation on clay strength", *Proceeding of the 11th International Conference on Soil Mechanics and Foundation Engineering*, San Francisco, California, U.S.A., August.

Meyerhof, G.G., Mathur, S.K. and Valsangkar, A.J. (1981), "Lateral resistance and deflection of rigid walls and piles in layered soils", *Can. Geotech. J.*, **18**(2), 159-170. https://doi.org/10.1139/t81-021.

Meyerhof, G.G., Sastry, V.V.R.N. and Yalcin, A.S. (1988), "Lateral resistance and deflection of flexible piles", *Can. Geotech. J.*, **25**(3), 511-522. https://doi.org/10.1139/t88-056.

Monismith, C.L.N.O. and Freeme, C.R. (1975), "Permenent deformation characteristics of subgrade soils due to repeated loading", *Proceedings of the 54th Annual Meeting of the Transportation Research Board*, Washington, U.S.A., January.

Narsilio, G.A. and Santamarina, J.C. (2008), "Terminal densities", *Geotechnique*, **58**(8), 669-674. https://doi.org/10.1680/geot.2008.58.8.669.

Niemunis, A., Wichtmann, T. and Triantafyllidis, T. (2005), "A high-cycle accumulation model for sand", *Comput. Geotech.*, **32**(4), 245-263. https://doi.org/10.1016/j.compgeo.2005.03.002.

Pasten, C., Shin, H. and Santamarina, J. (2014), "Long-term foundation response to repetitive loading, *J. Geotech. Geoenviron. Eng.*, **140**(4), 04013036. https://doi.org/10.1061/(ASCE)GT.1943-5606.0001052.

Peng, J., Clarke, B.G. and Rouainia, M. (2011), "Increasing the resistance of piles subject to cyclic lateral loading", *J. Geotech. Geoenviron. Eng.*, **137**(10), 977-982. https://doi.org/10.1061/(ASCE)GT.1943-5606.0000504.

Poulos, H.G. and Davis, E.H. (1980), *Pile Foundation Analysis and Design*, John Wiley & Sons, New York, U.S.A.

Prasad, Y.V. and Chari, T. (1999), "Lateral capacity of model rigid piles in cohesionless soils", *Soil Found.*, **39**(2), 21-29. https://doi.org/10.3208/sandf.39.2_21.

Randolph, M.F. (1981), "The response of flexible piles to lateral loading", *Géotechnique*, **31**(2), 247-259. https://doi.org/10.1680/geot.1981.31.2.247.

Reese, L.C. and Cox, W.R. (1975), "Field testing and analysis of laterally loaded piles in stiff clay", *Proceeding of the 7th Annual Offshore Technology Conference*, Offshore Technology Conference, Houston, Texas, U.S.A., May.

Reese, L.C., Cox, W.R. and Koop, F.D. (1974), "Analysis of laterally loaded piles in sand", *Proceeding of the 6th Annual Offshore Technology Conference*, Houston, Texas, U.S.A., May.

Sawczuk, A. (1974), "Shakedown analysis of elastic-plastic structures", *Nucl. Eng. Des.*, **28**(1), 121-136. https://doi.org/10.1016/0029-5493(74)90091-0.

Sawicki, A. (1994), "Elasto-plastic interpretation of oedometric test", *Arch. Hydro-Eng. Environ. Mech.*, **41**(1-2), 111-131.

Sawicki, A. and Swidzinski, W. (1995), "Cyclic compaction of soils, grains and powders", *Powder Technol.*, **85**(2), 97-104. https://doi.org/10.1016/0032-5910(95)03013-Y.

Sharp, R. and Booker, J. (1984), "Shakedown of pavements under moving surface loads", *J. Transport. Eng.*, **110**(1), 1-14. https://doi.org/10.1061/(ASCE)0733-947X(1984)110:1(1).

Shi, J., Zhang, Y., Chen, L. and Fu, Z. (2018), "Response of a laterally loaded pile group due to cyclic loading in clay", *Geomech. Eng.*, **16**(5), 463-469. https://doi.org/10.12989/gae.2018.16.5.463.

Smith, T.D. (1987), "Pile horizontal soil modulus values", *J. Geotech. Eng.*, **113**(9), 1040-1044. https://doi.org/10.1061/(ASCE)0733-9410(1987)113:9(1040).

Stewart, H.E. (1986), "Permanent strains from cyclic variable-amplitude loadings", *J. Geotech. Eng.*, **112**(6), 646-660. https://doi.org/10.1061/(ASCE)0733-9410(1986)112:6(646).

Suiker, A.S.J. and de Borst, R. (2003), "A numerical model for the cyclic deterioration of railway tracks", *Int. J. Numer. Meth.*

Eng., **57**(4), 441-470. https://doi.org/10.1002/nme.683.
Tiwari, B. and Al-Adhadh, A.R. (2014), "Influence of relative density on static soil–structure frictional resistance of dry and saturated sand", *Geotech*. *Geol*. *Eng*., **32**(2), 411-427. https://doi.org/10.1007/s10706-013-9723-6.
Tuladhar, R., Maki, T. and Mutsuyoshi, H. (2008), "Cyclic behavior of laterally loaded concrete piles embedded into cohesive soil", *Earthq*. *Eng*. *Struct*. *Dyn*., **37**(1), 43-59. https://doi.org/10.1002/eqe.744.
Wichtmann, T. (2005), "Explicit accumulation model for non-cohesive soils under cyclic loading", Ph.D. Dissertation, Ruhr-University Bochum, Bochun, Germany.
Wichtmann, T., Niemunis, A. and Triantafyllidis, T. (2005), "Strain accumulation in sand due to cyclic loading: Drained triaxial tests", *Soil Dyn*. *Earthq*. *Eng*., **25**(12), 967-979. https://doi.org/10.1016/j.soildyn.2005.02.022.
Wichtmann, T., Niemunis, A. and Triantafyllidis, T. (2007), "Strain accumulation in sand due to cyclic loading: Drained cyclic tests with triaxial extension", *Soil Dyn*. *Earthq*. *Eng*., **27**(1), 42-48. https://doi.org/10.1016/j.soildyn.2006.04.001.
Wichtmann, T., Niemunis, A. and Triantafyllidis, T. (2010a), "Strain accumulation in sand due to drained cyclic loading: On the effect of monotonic and cyclic preloading (Miner's rule)", *Soil Dyn*. *Earthq*. *Eng*., **30**(8), 736-745. https://doi.org/10.1016/j.soildyn.2010.03.004.
Wichtmann, T., Niemunis, A. and Triantafyllidis, T. (2010b), "On the determination of a set of material constants for a high-cycle accumulation model for non-cohesive soils", *Int*. *J*. *Numer*. *Anal*. *Meth*. *Geomech*., **34**(4), 409-440. https://doi.org/10.1002/nag.821.
Zhang, L., Silva, F. and Grismala, R. (2005), "Ultimate lateral resistance to piles in cohesionless soils", *J*. *Geotech*. *Geoenviron*. *Eng*., **131**(1), 78-83. https://doi.org/10.1061/(ASCE)1090-0241(2005)131:1(78).

IC